

Full text at publisher

Export

Add To Marked List

High-quality AlN growth: a detailed study on ammonia flow

By Yolcu, G (Yolcu, Gamze) ^{[1], [2]}; Koçak, MN (Kocak, Merve Nur) ^{[1], [2]}; Ünal, DH (Unal, Dudu Hatice) ^{[1], [3]}; Altuntas, I (Altuntas, Ismail) ^{[1], [3]}; Horoz, S (Horoz, Sabit) ^{[1], [4]}; Demir, I (Demir, Ilkay) ^{[1], [3]}

Source JOURNAL OF MATERIALS SCIENCE-MATERIALS IN ELECTRONICS

Volume: 34 Issue: 4
DOI: 10.1007/s10854-022-09556-0

Article Number 250

Published FEB 2023

Indexed 2023-03-02

Document Type Article

Jump to [↓ Enriched Cited References](#)

Abstract High crystalline and optical quality aluminum nitride (AlN) films with thin thickness have been grown on Al₂O₃ by MOVPE (metal-organic vapor phase epitaxy) and the NH₃ flow rate has been changed to improve the morphology and quality of the films. Some characterization types of equipment such as atomic force microscopy (AFM), high-resolution X-ray diffraction (HRXRD), and Raman spectroscopy have been carried out to investigate the effect of different NH₃ flow rates on surface morphology, roughness, and crystal quality of AlN, respectively. Unlike in the literature, in situ optical reflectance measurements have been given depending on NH₃ flow rate and optical characterization has been performed by UV-VIS-NIR spectrophotometry. The well-defined interference patterns in the optical transmittance graph report a sharp interface between AlN and Al₂O₃. Also, all obtained samples have a sharp absorption edge that shows the quality of the films, but Sample B with 900 sccm NH₃ flow has the sharpest absorption edge

Citation Network

In Web of Science Core C

2 Citations

Create citation alert

2 Times Cited in All D
+ See more times cited

59 Cited References
View Related Records

Citing items by classifi

Breakdown of how this item is mentioned, based on average context data and snippet item(s).

Background 0

Basis 0

Journal information

JOURNAL OF MATERIALS SCIENCE-MATERIALS IN ELECTRONICS

Publisher name: SPRINGER

Journal Impact Factor™

2.8

2022

2.5

Five Year

JCR Category	Category Rank	Category Quartile
ENGINEERING, ELECTRICAL & ELECTRONIC <i>in SCIE edition</i>	137/275	Q2
MATERIALS SCIENCE, MULTIDISCIPLINARY <i>in SCIE edition</i>	201/344	Q3
PHYSICS, APPLIED <i>in SCIE edition</i>	75/160	Q2
PHYSICS, CONDENSED MATTER <i>in SCIE edition</i>	34/67	Q3

Source: Journal Citation Reports 2022. [Learn more](#)

Journal Citation Indicator™

0.54

2022

0.51

2021

JCI Category	Category Rank	Category Quartile
ENGINEERING, ELECTRICAL & ELECTRONIC	137/275	Q2



High-quality AlN growth: a detailed study on ammonia flow

Gamze Yolcu^{1,2}, Merve Nur Koçak^{1,2}, Dudu Hatice Ünal^{1,3}, Ismail Altuntas^{1,3}, Sabit Horoz^{1,4}, and Ilkay Demir^{1,3,*} 

¹Nanophotonics Research and Application Center, Sivas Cumhuriyet University, 58140 Sivas, Turkey

²Department of Metallurgical and Materials Engineering, Faculty of Engineering Sivas, Cumhuriyet University, 58140 Sivas, Turkey

³Department of Nanotechnology Engineering, Faculty of Engineering, Sivas Cumhuriyet University, 58140 Sivas, Turkey

⁴Department of Metallurgical and Materials Engineering, Faculty of Engineering and Natural Sciences, Sivas University of Science and Technology, 58140 Sivas, Turkey

Received: 17 August 2022

Accepted: 21 November 2022

Published online:

25 January 2023

© The Author(s), under exclusive licence to Springer Science+Business Media, LLC, part of Springer Nature 2023

ABSTRACT

High crystalline and optical quality aluminum nitride (AlN) films with thin thickness have been grown on Al₂O₃ by MOVPE (metal-organic vapor phase epitaxy) and the NH₃ flow rate has been changed to improve the morphology and quality of the films. Some characterization types of equipment such as atomic force microscopy (AFM), high-resolution X-ray diffraction (HRXRD), and Raman spectroscopy have been carried out to investigate the effect of different NH₃ flow rates on surface morphology, roughness, and crystal quality of AlN, respectively. Unlike in the literature, in situ optical reflectance measurements have been given depending on NH₃ flow rate and optical characterization has been performed by UV–VIS–NIR spectrophotometry. The well-defined interference patterns in the optical transmittance graph report a sharp interface between AlN and Al₂O₃. Also, all obtained samples have a sharp absorption edge that shows the quality of the films, but Sample B with 900 sccm NH₃ flow has the sharpest absorption edge because it has high optical quality and low defect. The RMS (root mean square), D_S (screw-type dislocation density), and D_E (edge-type dislocation density) values of AlN with 900 sccm NH₃ flow are 0.22 nm, 7.86×10^7 , and $1.68 \times 10^{10} \text{ cm}^{-2}$, respectively. The results obtained are comparable to the literature.

1 Introduction

AlN (aluminum nitride) has direct wide bandgap (6.2 eV), high resistance (10^{11} – $10^{13} \Omega \text{ cm}$), high piezoelectric coefficient ($d_{33} = 5.56$), high hardness

(12 GPa for the (0001) plane), and good thermal conductivity (285 W / mK) [1–5]. Since AlN has unique properties, it has many different application areas, for example, ultraviolet photodetectors, light-emitting diodes (LED), quantum cascade lasers

Address correspondence to E-mail: idemir@cumhuriyet.edu.tr

(QCL), radio frequency filters, micro-electro-mechanical systems, and solar cells [6–15]. Moreover, AlN is used as a buffer layer for GaN (the most studied extensively III-nitride semiconductor) growth on Si. The main reason behind the use of a buffer layer prevents the occurring reaction, called meltback etching, between GaN and Si at high temperatures when GaN is grown directly on Si [16–21]. The quality of the AlN film has an important place in the performance or efficiency of the device to be produced [22]. However, many difficulties are encountered since AlN is grown on substrates such as Si and Al₂O₃ due to the cost of the AlN substrate. The substantial discrepancy in the thermal expansion coefficient and the high lattice mismatch between the substrate and the AlN are two of these challenges [23, 24]. Important growth problems including the poor mobility of Al adatoms and parasitic interactions between precursors should also be taken into account [25]. However, a variety of methods have been employed to reduce the impact of current issues and produce AlN films with good crystal quality. Here, a few of them that can be mentioned as follows: In order to decrease the dislocation density and produce a film without cracks, patterned substrates are employed [26–28]. The quality of the produced film depends on many parameters and can be controlled. The mechanism of problems such as anti-phase boundaries, threading dislocations, and stacking faults is discussed and miscut Si substrate, buffer layers, thermal annealing, and epitaxial lateral overgrowth methods are suggested to suppress them [29]. Studies in the literature indicated that parasitic reactions decreased with the use of the pulsed atomic-layer epitaxy (PALE) technique and the crystal quality of the film changed with the change in the V/III ratio [30, 31]. In addition, a study has been reported about the growth of low temperature (LT) and high temperature (HT) layers like sandwiches combined with PALE MOVPE. Surface morphology and crystal quality are significantly improved with this method [32].

It is well known in the literature that the parasitic reaction between TMAI (trimethylaluminum) and NH₃ (ammonia) is one of the major factors negatively affecting the quality of AlN. The effects of the undesired mechanism between TMAI-NH₃ have been presented in detail. It has been shown that when there is sufficient TMAI flow as the NH₃ flow increases, the parasitic reactions in the gas phase

increase, and the growth rate decreases [33]. It has been also demonstrated that as the parasitic reactions increase, the surface becomes rougher [34, 35]. The appearance of white particles on the reactor sidewalls proves the parasitic reactions between TMAI and NH₃ [10, 36]. In other words, large grains are formed at high NH₃ flow, and V-pits are formed as a result of the large grains, not coalescence, that is, high NH₃ leads to 3D growth mode, not 2D [37, 38]. The effect of the NH₃ flow can also be considered in terms of the V/III ratio. The morphologies of AlN films with high and low NH₃ flow rates are shown schematically in the literature. The high NH₃ flow causes the dominant N polarity and the surface becomes rough due to the inversion fields formed. Not only high NH₃ flow but also low one negatively affects the film, and low NH₃ results in thin films with feather-like properties [39]. Although the parasitic reactions between TMAI and NH₃ that promote the formation of AlN nanoparticles in the gas phase are well known and can be identified by modeling, the mechanisms affecting surface morphology are still undefined [38, 40].

In this study, AlN films have been grown on Al₂O₃ using the PALE technique to prevent parasitic reactions and high growth temperature has been used to increase the mobility of Al adatoms. After all the growth parameters have been optimized, it has been investigated the effect of just the ammonia flow rate change on the film. Adopting adjusted NH₃ flow rates during the growth process is also intended to improve the quality of the AlN while reducing the impact of the parasitic reaction. The use of different NH₃ flow rates has been shown to improve the quality of the AlN using a variety of characterization tools. Unlike previous studies [28, 30, 35, 37–39], we have given in situ optical reflectance measurements used for control of the epitaxial film surface and growth rate during growth. Moreover, the effect of NH₃ flow rate on optical quality has been investigated with transmittance and absorbance measurements by UV–VIS–NIR spectrophotometry after growth.

2 Experimental

The epitaxial AlN films have been grown on Al₂O₃ by using MOVPE reactor, AIXTRON 200/4 RF-S horizontal flow. TMAI and NH₃ precursors have been

used to obtain Al and N sources, respectively. Before the growths, in situ high temperature (~ 1100 °C) desorption has been exposed for ~ 10 min for thermal cleaning. Following this, an AlN nucleation layer has been grown at 1080 °C for 10 min with flows of TMAI = 14 sccm and NH_3 = 1200 sccm. Subsequently, AlN films have been grown with the PALE growth method that prevents parasitic reactions at a temperature of 1440 °C by feeding the TMAI and NH_3 precursors for 4 and 2 s (600 loops), by turn. Four AlN samples (A-D) have been grown with different NH_3 flow rates (750, 900, 1050, and 1200 sccm) while the TMAI flow rate has been fixed to 77 sccm. In situ optical reflectance with a monitoring wavelength of 880 nm has been utilized to control important parameters such as growth rate and surface quality during the growths. HRXRD (Rigaku SmartLab), AFM (Hitachi AFM 5100 N) in dynamic force mode, UV-VIS-NIR spectrophotometry (Varian Cary 5000), and Raman spectroscopy (Witec) have been used for the characterization of samples to examine the impact of NH_3 flow rate on dislocation density, surface morphology, and in-plane stress properties of AlN.

3 Results and discussion

In situ optical reflectance measurements have been done to control the growth condition of AlN films. The in situ optical reflectance curves for Samples A, B, C, and D are displayed in Fig. 1. AlN's greater refractive index than Al_2O_3 causes its reflectance to behave more favorably [41]. The amplitude of the reflectance curves is almost the same, indicating that the NH_3 flow rate does not optically overly affect the surface property [42]. Start-min and max/min measurements are plotted against NH_3 flow in Fig. 2. The difference between the starting and minimum values of in situ reflectance measurements is known as the start-min values. The in situ reflectance's maximum and minimum values are represented by the max/min values. Surface roughness is determined by the difference between the in situ reflectance's starting and minimum points [9]. It is expected that the max/min value is high, which is the determination of optical quality while the start-min value is low, which is the determination of surface roughness. Sample B and Sample C are better than other samples in terms of these values. In situ reflectance

measurement only gives us an opinion and it is not enough to check the quality of sample. For this reason, it should be supported by ex situ characterization techniques such as AFM and UV-VIS-NIR spectrophotometry. In this study, we discuss in more detail the results of AFM and UV-VIS-NIR spectrophotometry.

X-ray rocking curve measurement has been carried out to examine the effect of the amount of NH_3 flow on the crystal quality of AlN films. It has been reported that symmetric (002) and asymmetric (102) rocking curves are affected by D_S and dominantly D_E , respectively [43]. The symmetric and asymmetric rocking curve measurements of AlN films obtained with HRXRD are shown in Figs. 3 and 4, respectively. As is clearly shown in Fig. 3, the symmetric rocking curve peaks of AlN films with high and low NH_3 flow rates are broad. In general, the symmetric omega peak broadening is expected to decrease significantly when the growth mode is changed to 2D growth [43]. Sample B and Sample C have been considered to have 2D growth modes because of their narrow symmetric omega peaks. On the other hand, the asymmetric peaks are close to each other according to the symmetric omega peaks.

Defects in crystals often cause the surface to twist or tilt. Tilt is the deviation of the grain growth direction from the c-axis. Tilt introduces screw dislocations parallel to the growth direction and broadens the full width at half-maximum (FWHM) values of symmetric omega. Twist is the c-axis torsion, introduces edge dislocations parallel to the growth direction, and broadens the FWHM values of asymmetric omega. Thus, the FWHM values of the rocking curve can be used to characterize the quality of the crystal [44]. The variation of FWHM values obtained from symmetric and asymmetric omega measurements is given in Fig. 5. Considering the symmetric omega FWHM values, it is seen that Sample A has the max and Sample C has the min. FWHM of Sample A and Sample C is 886 arcsec and 117 arcsec, respectively. On the contrary, regarding the asymmetric omega FWHM values given in Fig. 5, it is seen that Sample C has the highest and Sample D has the lowest FWHM value. The FWHM values of

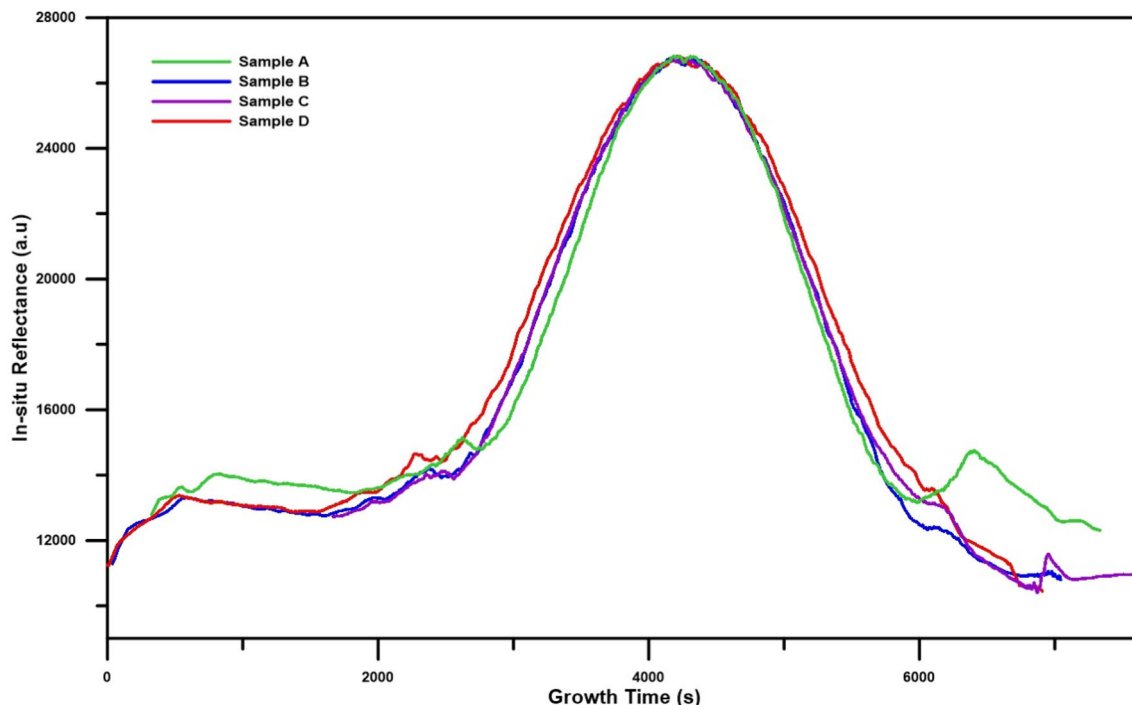


Fig. 1 In situ optical reflectance curves obtained from AlN growth of Sample A, B, C, and D

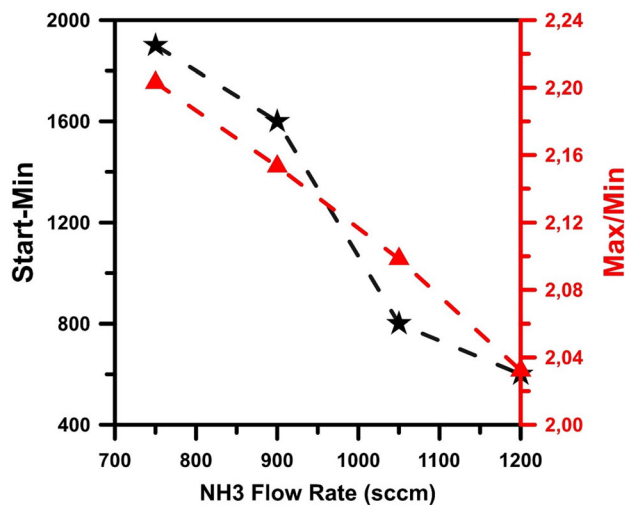


Fig. 2 The variation of Max/Min and Start-Min values of Sample A, B, C, and D with the changing of NH_3 flow rate

Sample C and Sample D are 2006 and 1518 arcsec, respectively. The difference between the symmetric omega values of the samples is large while the asymmetric omega FWHM values are close to each other.

FWHM values of symmetric and asymmetric omega scans are widely used to calculate the dislocation density mainly including D_S and D_E . D_S and D_E are related to FWHM values of symmetric and

asymmetric omega scans, respectively [45]. The following equations give the dislocation densities:

$$D_S = \frac{\beta_{002}^2}{4.35b_S^2}$$

$$D_E = \frac{\beta_{102}^2}{4.35b_E^2}$$

where $b_S = 0.4982$ nm and $b_E = 0.3112$ nm are the Burgers vector sizes and β_S and β_E correspond for FWHM values of symmetric and asymmetric omega scans, respectively. D_S for samples A, B, C, and D has been calculated as 1.71×10^9 , 7.86×10^7 , 2.98×10^7 , and 9.40×10^8 cm^{-2} , respectively. D_E for samples A, B, C, and D has been calculated as 1.29×10^{10} , 1.68×10^{10} , 2.25×10^{10} , and 1.28×10^{10} cm^{-2} , respectively. The calculated D_E are very close to each other. However, there are significant differences in the calculated D_S . Sample A has the largest value and Sample C has the smallest value. XRD analysis results and calculated TDD (threading dislocation densities) for all samples grown in different NH_3 flow rates are given in Table 1. It can be said that samples B and C have a low density of D_S but the dominant dislocation in the film is D_E caused by the large lattice mismatch between the AlN and the Al_2O_3 [45].

Fig. 3 Symmetric (002) omega measurements of Sample A, B, C, and D

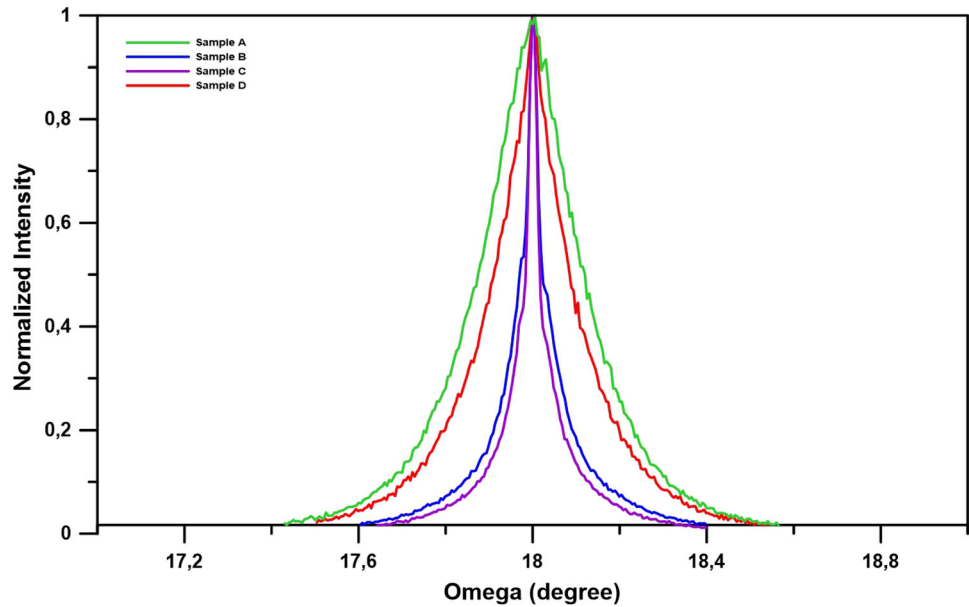
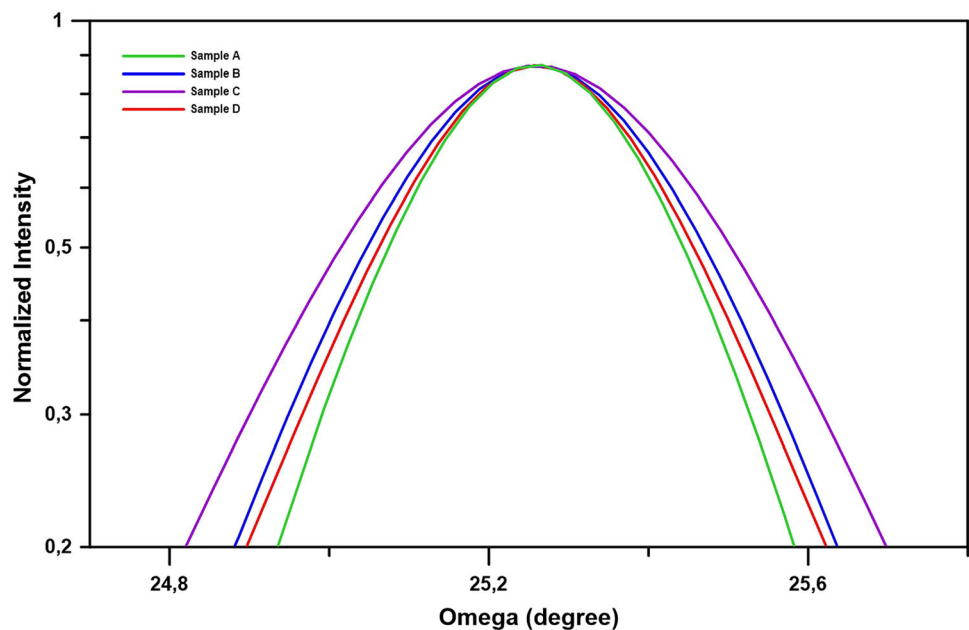


Fig. 4 Asymmetric (102) omega measurements of Sample A, B, C, and D



In more detail, generally dislocations produced at the boundaries of nucleation islands are edge type, while dislocations starting inside the islands are screw type. Fewer but larger islands tend to form when the ammonia flow is low. Islands may grow both laterally and vertically (3D). There is enough time for these islands to coalesce, but as can be seen from the RMS values, the dislocations cannot come together and cannot annihilate each other due to the height difference of the islands. Even if grown AlN on c-sapphire with optimum ammonia flow, the

islands may be twisted together as they coalesce, and edge dislocations occur. On the other hand, screw-type dislocations bend during lateral growth and can come together and annihilate each other. Although it is expected that the edge and screw dislocations will decrease and increase together, there are many studies in the literature in which the edge dislocation increases while the screw dislocation decreases [37]. Many but small islands are formed due to the small mobility of the Al adatom when the ammonia flow is too high. Since there is not much space between the

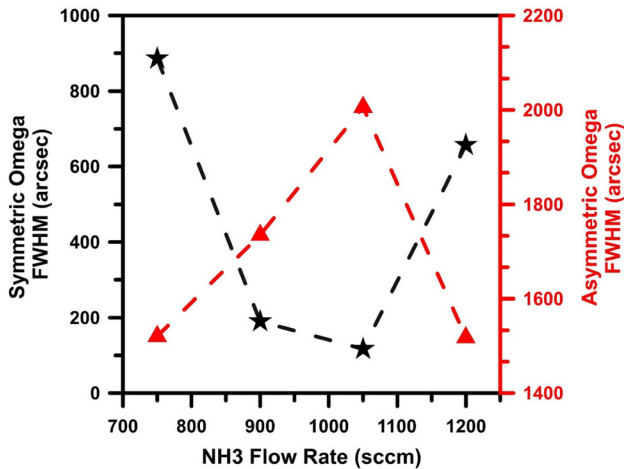


Fig. 5 FWHM value obtained from symmetric and asymmetric omega measurements of Sample A, B, C, and D

islands, there is little lateral growth time and not enough time for the screw dislocations to annihilate each other.

In addition to dislocation density, strain and biaxial stress calculations were made using symmetric and asymmetric omega measurements. Firstly, using Bragg’s law ($n\lambda = 2d_{hkl}\sin \theta$), angle θ is determined to obtain the distance d_{hkl} between a certain set of planes.

The lattice parameters a and c of the hexagonal AlN film are found by the following equation.

$$d_{hkl} = \frac{1}{\sqrt{\frac{4}{3} \frac{h^2+k^2+hk}{a^2} + \frac{l^2}{c^2}}}$$

It is sufficient to use the (002) plane to calculate the c -parameter with this equation, but another plane (here the (102) plane) should be used to find the a -

parameter. The accuracy of these calculations depends on the accuracy of the measurement, although it may contain a small margin of error. First, c -parameter is found and since there is a -parameter dependent on c -parameter, the error margin of a -parameter is larger. Since the AlN films are grown by the heteroepitaxy method, the lattice may undergo deformation, and to see this, strain calculation is made using the lattice parameter. The in-plane (ϵ_{xx}) and out-of-plane (ϵ_{zz}) strain can be calculated with the equations given below ($c_0 = 0.49792$ and $a_0 = 0.31114$ nm for the strain-free AlN).

$$\epsilon_{xx} = \frac{a_{meas} - a_0}{a}$$

$$\epsilon_{zz} = \frac{c_{meas} - c_0}{c}$$

After that, the equations given below were used in the calculation of the biaxial and hydrostatic strain components.

$$\epsilon_{xx}^{(b)} = \epsilon_{xx} - \epsilon_h$$

$$\epsilon_{zz}^{(b)} = \epsilon_{zz} - \epsilon_h$$

$$\epsilon_h = \frac{1 - \nu}{1 + \nu} \left(\epsilon_{zz} + \frac{2\nu}{1 - \nu} \epsilon_{xx} \right)$$

$$\nu = \frac{c_{13}}{c_{13} + c_{33}}$$

$\epsilon_{xx}^{(b)}$, $\epsilon_{zz}^{(b)}$, ϵ_h and ν have given in the above equations represent biaxial (in the a -direction and in the c -direction), hydrostatic strains, and Poisson ratio, respectively. Poisson ratio has a wide variation as it depends on the chosen elastic constants. Calculated values are given in Table 1. While in-plane strain is compressive, out-of-plane strain is tensile. Sample C

Table 1 XRD analysis results, TDD, and the biaxial and hydrostatic strain components at different NH₃ flow rates

Sample	PALE NH ₃ (sccm)	FWHM omega 002 (arcsec)	FWHM omega 102 (arcsec)	D _s (cm ⁻²)	D _E (cm ⁻²)	ϵ_{xx} (10 ³)	ϵ_{zz} (10 ⁴)	ϵ_h (10 ³)	σ_f (GPa)
Sample A	750	886	1521	1.71×10^9	1.29×10^{10}	-29.14	5.93	-10.64	7.34
Sample B	900	190	1735	7.86×10^7	1.68×10^{10}	-28.15	9.21	-10.07	7.18
Sample C	1050	117	2006	2.98×10^7	2.25×10^{10}	-27.88	6.90	-10.10	7.06
Sample D	1200	657	1518	9.40×10^8	1.28×10^{10}	-28.53	6.58	-10.37	7.21

has the lowest in-plane strain and Sample A is the highest. On the other hand, Sample B has the highest, and Sample A has the lowest out-of-plane strain.

In-plane biaxial stress (σ_f) occurs due to lattice mismatch, growth conditions, and difference in thermal expansion coefficients between film and substrate. In-plane biaxial stress is calculated by the equation given below and c_{11} , c_{12} , c_{13} , and c_{33} elastic modulus values are taken as 345, 125, 120, and 395 GPa, respectively.

$$\sigma_f = \left[c_{11} + c_{12} - 2 \frac{c_{13}^2}{c_{33}} \right] \varepsilon_{xx}^{(b)}$$

Although the calculated in-plane biaxial stress values are close to each other, Sample C has the lowest value, followed by Sample B.

AFM images of $5 \mu\text{m} \times 5 \mu\text{m}$ area of all samples are indicated in Fig. 6a–d. The RMS surface roughness values of Sample A–D on an area of $5 \mu\text{m} \times 5 \mu\text{m}$ are 7.30, 0.22, 2.27, and 0.16 nm, respectively. When AFM images are examined, it has observed in 3 dimensions growth mode and islands in Fig. 6a. However, in Fig. 6b, the islands coalesced and there are a few surface pits. When the NH_3 flow rate has been kept increasing, it is observed that the islands coalesce in Sample C and more surface pits are formed compared to Sample B. It is known that the coalescence time is dependent on the amount of NH_3 , as the NH_3 is reduced, the islands begin to coalesce with each other. An increase in roughness is most likely regarding long-term coalescence [45, 46]. It is seen that as the NH_3 flow increases, the surface roughness also increases [47]. Small size islands with high density are seen in Fig. 6d. It has been proved by the AFM technique in the studies that smaller islands are formed with the further increase of the NH_3 flow rate (the V/III ratio). The formation of small islands in Sample D can be attributed to the excessive increase in NH_3 flow [48]. It can be said that the film with the smoothest surface is Sample B. This is based on the increasing dominance of Al-polarity with the reduction of the NH_3 flow rate induced by the N polarity [47]. The surface and strain energy of the film affect the morphology of the surface. The wrinkling and buckling of thin film create high and low strain energies. The strain energies are related to the mass transfer process in the thin film [49]. The smaller stress corresponds to wrinkles with a larger

wavelength. As the Al fraction on Al_2O_3 increases, the wavelength of the surface oscillations increases, resulting in a smoother surface [39]. On the other hand, the surface roughness increased when the NH_3 flow rate has been reduced to 750 sccm. It is estimated AlN films grown with PALE form whisker-like structures [49]. In Fig. 6e–h, 3D AFM images of the $2 \mu\text{m} \times 2 \mu\text{m}$ area of all samples are given. The RMS values of Sample A–D on an area of $2 \mu\text{m} \times 2 \mu\text{m}$ are 7.19, 0.29, 4.34, and 0.30 nm, respectively. As mentioned above, it is seen more clearly the existence of the islands when looking at Fig. 6e and the islands coalescence and smooth surface are obtained in Fig. 6f. Also, surface pits in Fig. 6g and small islands in Fig. 6h are very evident.

The schematic representations of AlN film grown on the Al_2O_3 at different NH_3 flow rates are given in Fig. 7. The film has been formed layer by layer with an optimum NH_3 flow rate. On the contrary, the Al atoms are stacked on top of each other with a low NH_3 flow rate, and the Al atoms cluster with a high NH_3 flow rate.

An optical transmittance graph is obtained by the interference of reflections from the film surfaces and the interfaces between the film and substrate [50, 51]. The optical transmittance versus wavelength graph for samples is shown in Fig. 8. It is seen that the average transmittance of all films for the wavelength larger than 250 nm wavelength is above 75%. AlN films show high optical transparency in the UV–visible region.

The well-defined interference patterns in the optical transmittance graph report a sharp interface between AlN thin films and Al_2O_3 [52]. The shift of the optical absorption edge shows that the quality of the films changes; in other words, the surface roughness and the defect density can increase the scattering of the incident light and cause a decrease in transmittance [53–55]. All samples have a sharp absorption edge, but Sample B has the sharpest absorption edge. The sharp drop in the absorption edge of Sample B at 900 sccm of NH_3 flow and interference patterns show that Sample B has the highest optical quality. Considering the transmittance level, it has been thought that the number of defects causing light scattering and absorption decreased as the NH_3 flow rate increased from 750 sccm to 900

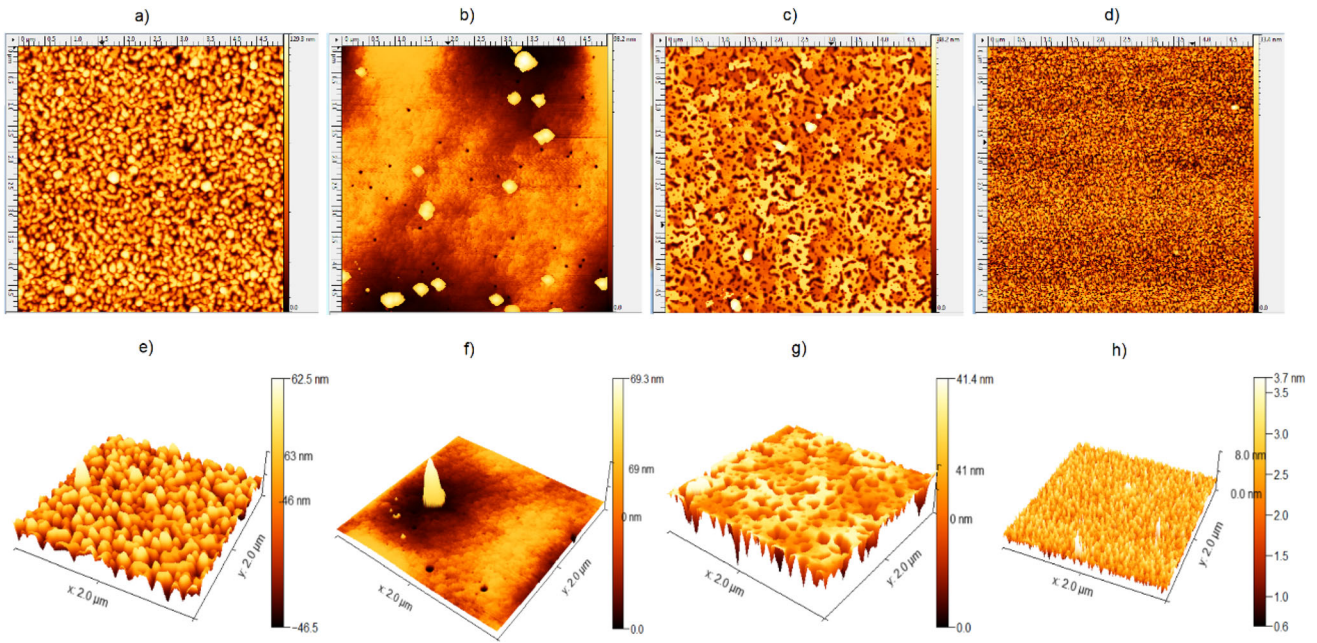


Fig. 6 The AFM topography images of the surface of Sample A (a, e), B (b, f), C (c, g), and D (d, h). a–d AFM scanning images of 5 μm × 5 μm area and (f–h) 3D AFM scanning images of 2 μm × 2 μm area

Fig. 7 Schematic diagram of grown AlN films with a optimum b low and c high NH₃ flow rate

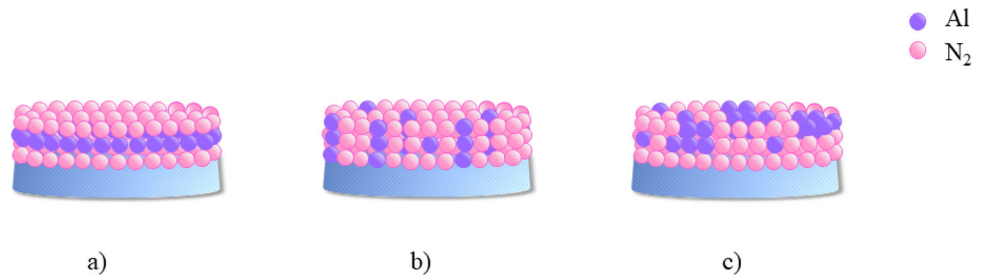
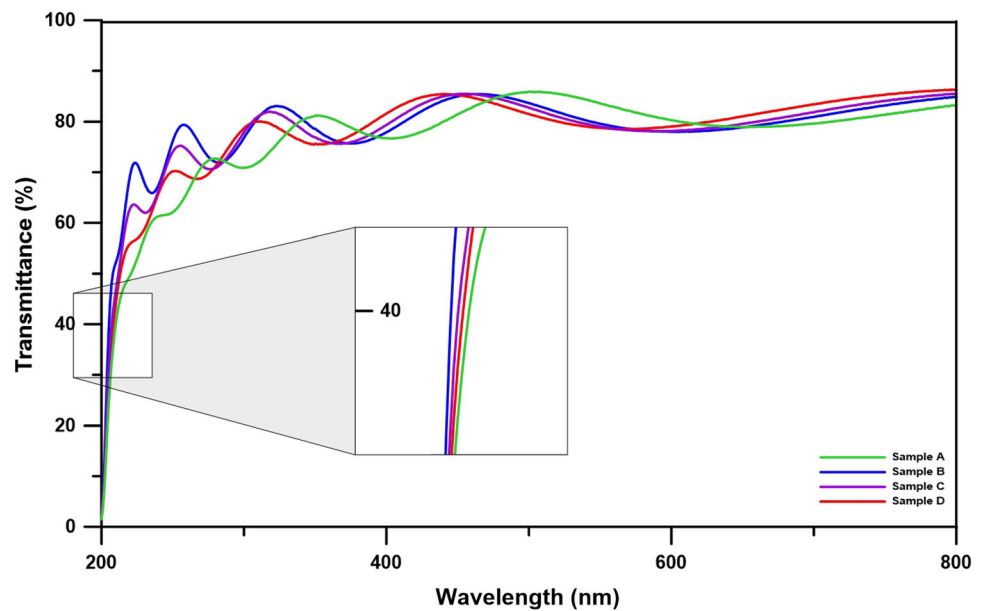


Fig. 8 The optical transmittance versus wavelength plots for the AlN films at room temperature



scm, but these defects increased when the NH₃ flow rate has been increased above 900 scm. Our spectrophotometry results are very compatible with AFM results. It can be said that Sample B has a high transmittance level because it has the smoothest surface. Sample D may have a low RMS value, but transmittance is low due to having many small islands on its surface.

The plot of $(\alpha h\nu)^2$ versus photon energy ($h\nu$) is given in Fig. 9, and the linear extrapolations to the photon energy axis in the inset graph are shown. The optical bandgap (E_g) of the AlN films can be determined by linear extrapolations to the photon energy axis. The effective bandgaps of samples A-D are, respectively, about 6.12, 6.14, 6.12, and 6.12 eV. The enlargement of absorption band energy is proof of improved material quality [52]. The fact that the absorption band energy of Sample B is higher than other samples can be attributed to the quality.

Figure 10 shows the Raman spectra of Sample A, B, C, and D in the 200–1000 cm⁻¹ wavelength range (a) and the graphs of the Gaussian fit of the AlN-E2 (high) mode (b). Al₂O₃ Eg modes are around 750, 577, 378, 431, and 448 cm⁻¹, and Al₂O₃ A1g mode is in the range of 416–419 cm⁻¹. The AlN-E2 (high) mode peaks of the four samples have been seen, using the shift in the AlN-E2 peak to calculate the in situ compressive strain. The AlN-E2 mode peaks of samples A, B, C, and D are 659.37, 655.53, 658.22, and

658.22 cm⁻¹, respectively. The unstrained peak of the AlN-E2 (high) mode is taken as 657 cm⁻¹, and this wavelength is indicated as dashed in Fig. 10b [53]. The AlN-E2 (high) peak shifts to lower wavelengths or higher wavelengths indicating tensile or compressive strain.

The in-plane compressive stress can be calculated follow as:

$$\sigma = \frac{\lambda_R - \lambda_0}{K}$$

where $\lambda_R - \lambda_0$ and K are the phonon peak shift and the pressure coefficient (4.3 cm⁻¹ GPa⁻¹), respectively [54].

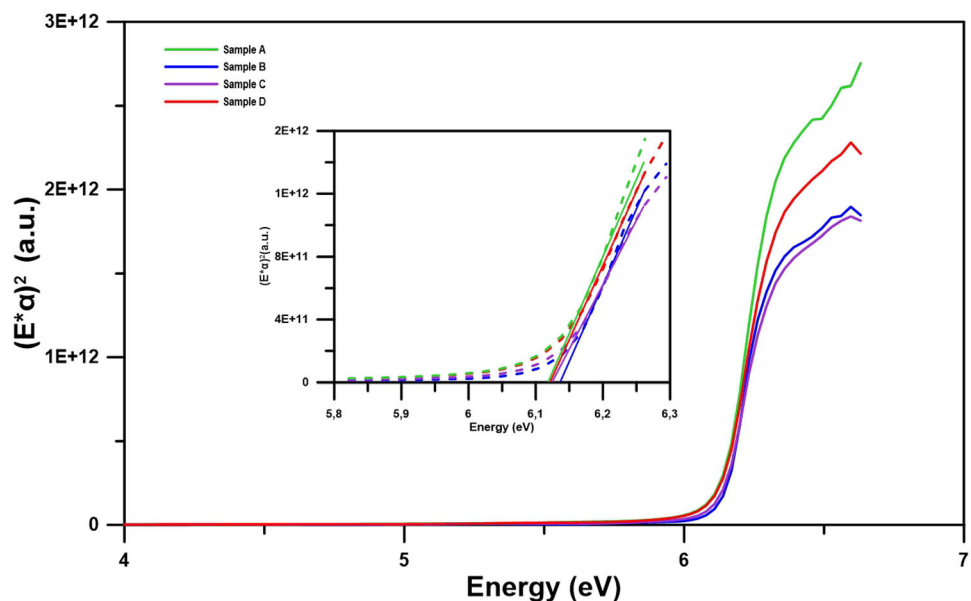
The in-plane compressive strain can be calculated as follows:

$$\varepsilon = \frac{\sigma}{Y}$$

where σ and Y are the in-plane compressive stress and the biaxial stress of AlN (469 GPa) [55].

The calculated and presented in Table 2 in-plane stress and strain values are consistent with the studies in the literature. In Table 2, the stress obtained with XRD and Raman spectroscopy is given in GPa. A large difference has been observed between the results from XRD and Raman spectroscopy. Although this has been unexpected at first, it was observed that they encountered similar discrepancies when the studies in the literature have been examined, it was observed that they encountered similar

Fig. 9 The change of $(E * \alpha)^2$ versus energy and enlarged band gap peaks (inset graph) of samples grown with the different NH₃ flow rates



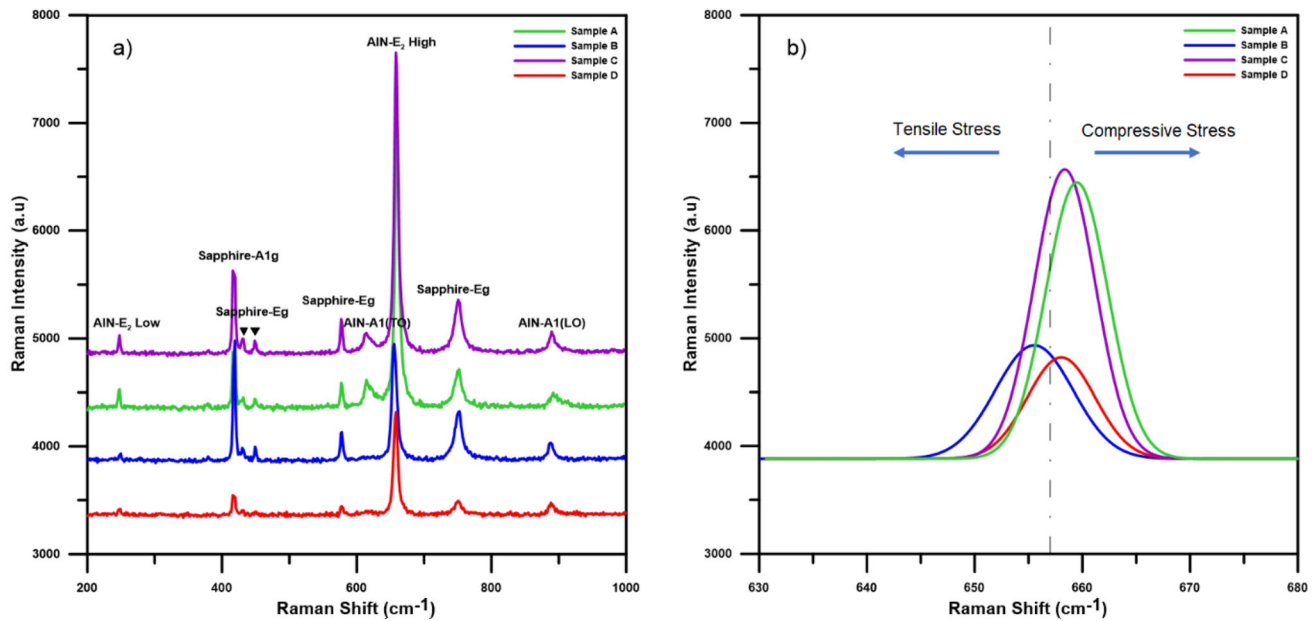


Fig. 10 a Raman spectra for AIN films with various NH_3 flow rates deposited on Al_2O_3 and b Gaussian fit graph of the AIN-E2

discrepancies. Given that stress cannot be measured directly, these discrepancies were thought to be due to the physics of the technique used. Changes in the spacing of the lattice planes take place due to deformation. Therefore, x-ray diffraction method takes advantage of the crystal structure, using the lattice spacing as a stress gauge. Reference parameters such as the strain-free AIN lattice parameters, Poisson value, and elastic modules affect the stress value while calculating with XRD. Raman scattering can be used to obtain structural information and properties of crystals from vibrational transitions. Raman peak shift relative to the unstressed position provides information about the stress present in the samples. Unlike X-ray, Raman scattering cannot detect dislocations and wafer bending. Although stress measurement with XRD is common in the literature, Raman spectroscopy has recently been used because it is stress sensitive. The stress values given by XRD are very close to each other. And for that reason, samples were compared considering the Raman

results. Sample B has tensile stress while other samples have compressive stress.

AIN A1 (LO) modes are less clear. In addition, the forbidden modes AIN A1 (TO) in the $z(xx)\bar{z}$ scattering configuration are seen in the Raman Spectra of A and C samples. This may be due to the roughness orientation of the AIN grains [56]. Stress causes rough surface and poor quality, thus revealing the forbidden AIN A1 (TO) mode in the Raman spectra of the samples [43]. The forbidden mode peak indicates that the crystal quality of Sample A and C is not as good as Sample B and D, which is identical to the results of XRD.

In Table 3, dislocation density and RMS values are given in order to compare this study with similar studies in the literature. It is known that RMS and XRD FWHM values of the AIN film improve with increasing thickness [46]. The thickness of Sample B has been found to be approximately 250 nm by using spectroscopic ellipsometry. The AIN film thicknesses given in Table 3 are larger than the thicknesses examined in this current study. However, we

Table 2 Calculated in-plane stress and strain at different NH_3 flow rates

	Stress from Raman (GPa)	Strain from Raman (%)	σ_f from XRD (GPa)
Sample A	- 0.551	- 0.117	- 7.34
Sample B*	0.342*	0.072*	- 7.18
Sample C	- 0.2835	- 0.060	- 7.06
Sample D	- 0.2835	- 0.060	- 7.21

Table 3 List of reported dislocation density and RMS of AlN films grown with the same growth techniques

AlN Film Thickness	RMS (nm)	D_s (cm ⁻²)	D_E (cm ⁻²)	References
1.4 μm	0.288	3.51×10^7	1.95×10^9	[46]
2.0 μm	1.61	1.50×10^7	3.70×10^9	[39]
250 nm	0.98	2.06×10^7	7.33×10^9	[57]
3.0 μm	–	0.66×10^8	7.97×10^8	[58]
~ 250 nm	0.22	7.86×10^7	1.68×10^{10}	This study

obtained dislocation density and RMS values are very close to the values in these studies.

4 Conclusion

To sum up, the effect of NH₃ flow rate on optical properties has been investigated for the first time by UV–VIS–NIR spectrophotometry. Obtained results are given together with the effects of NH₃ flow rate on crystal quality and surface morphology that have been analyzed with ex situ characterization methods such as HRXRD, AFM, and Raman. In the absence of sufficient NH₃ flow, it has been noticed that D_S , RMS value, and stress and strain values are high, and also the transmittance level is low. The islands formed on the surface coalescence and better crystal and optical quality have been obtained when the NH₃ flow has been increased to 900 sccm, so the flow has been accepted as the optimum NH₃ flow. For Sample B with the flow, the values of D_S and D_E are 7.86×10^7 and 1.68×10^{10} cm⁻², respectively. The AFM measurement shows a smooth surface with RMS of 0.22 nm and the transmittance spectrum of the AlN dropped sharply around the absorption bandgap of AlN. The film deteriorates both in terms of surface morphology and optical properties when the NH₃ flow increases further. By changing the amount of NH₃ flow, not only the crystal quality is increased, but also the surface morphology and optic properties improve. Although these samples have thinner thicknesses, the results obtained are comparable to thicker films in the literature.

Acknowledgements

The authors acknowledge the usage of the Nanophotonics Research and Application Center at Sivas Cumhuriyet University (CUNAM) facilities. This work is supported by both The Scientific and Technological Research Council of Turkey (TÜBİTAK, project number 118F425), and Cumhuriyet University Scientific Research Projects (CUBAP, project number M-2022-827).

Author contributions

GY participated in the conceptualization, investigation, and writing of the original draft. MNK, DHÜ, and SH participated in the investigation and writing – review & editing. IA participated in the investigation, formal analysis, and funding acquisition. ID participated in the funding acquisition, methodology, project administration, supervision, and writing – review & editing. All authors read and approved the final manuscript.

Data availability

Data can be available from the corresponding author upon academic reasonable request.

Declarations

Conflict of interest The authors declare that they have no conflict of interest. The submitted work is original and not has been published elsewhere in any form or language.

References

1. H. Yamashita et al., Optical properties of AlN epitaxial thin films in the vacuum ultraviolet region. *J. Appl. Phys.* **50**(2), 896–898 (1979)
2. M. Morita et al., Epitaxial growth of aluminum nitride on sapphire using metalorganic chemical vapor deposition. *Jpn. J. Appl. Phys.* **20**(1), 17 (1981)
3. Q. Hua et al., Aluminum, gallium, and indium nitrides (2020)
4. G.A. Slack et al., The intrinsic thermal conductivity of AlN. *J. Phys. Chem. Solids* **48**(7), 641–647 (1987)
5. M.-A. Dubois, P. Muralt, Stress and piezoelectric properties of aluminum nitride thin films deposited onto metal electrodes

- by pulsed direct current reactive sputtering. *J. Appl. Phys.* **89**(11), 6389–6395 (2001)
6. S. Guha, N.A. Bojarczuk, Ultraviolet and violet GaN light emitting diodes on silicon. *Appl. Phys. Lett.* **72**(4), 415–417 (1998)
 7. M.N. Abd Rahman, A. Shuhaimi, O.C. Seng, G. Tan, A. Anuar, N.A. Talik, ... W.H. Abd Majid, The crystallographic quality and band-edge transition of as-deposited PALE AlN films via metal organic chemical vapor deposition. *J. Mater. Sci.: Mater. Electron.* **32**(3), 3211–3221 (2021)
 8. D. Zhao et al., Surface morphology of AlN buffer layer and its effect on GaN growth by metalorganic chemical vapor deposition. *Appl. Phys. Lett.* **85**(9), 1499–1501 (2004)
 9. O. Reentilä et al., Effect of the AlN nucleation layer growth on AlN material quality. *J. Cryst. Growth.* **310**(23), 4932–4934 (2008)
 10. Y. Feng et al., Competitive growth mechanisms of AlN on Si (111) by MOVPE. *Sci. Rep.* **4**(1), 1–5 (2014)
 11. F. Semond, Epitaxial challenges of GaN on silicon. *MRS Bull.* **40**(5), 412–417 (2015)
 12. M. Mishra et al., Influence of metallic surface states on electron affinity of epitaxial AlN films. *Appl. Surf. Sci.* **407**, 255–259 (2017)
 13. B.T. Tran et al., High-quality AlN template grown on a patterned Si (111) substrate. *J. Cryst. Growth.* **468**, 225–229 (2017)
 14. S. Walde et al., AlN overgrowth of nano-pillar-patterned sapphire with different offcut angle by metalorganic vapor phase epitaxy. *J. Cryst. Growth.* **531**, 125343 (2020)
 15. I. Altuntas, M.N. Kocak, G. Yolcu, H.F. Budak, A.E. Kasapoğlu, S. Horoz, ... I. Demir, Influence of the PALE growth temperature on quality of MOVPE grown AlN/Si (111). *Mater. Sci. Semiconduct. Process.* **127**, 105733 (2021)
 16. A. Krost, A. Dadgar, GaN-based optoelectronics on silicon substrates. *Mater. Sci. Engineering: B* **93**(1–3), 77–84 (2002)
 17. W. Luo et al., Influence of AlN buffer layer thickness on the properties of GaN epilayer on Si (1 1 1) by MOCVD. *Microelectron. J.* **39**(12), 1710–1713 (2008)
 18. D. Zhu et al., Prospects of III-nitride optoelectronics grown on Si. *Rep. Prog. Phys.* **76**(10), 106501 (2013)
 19. P.-J. Lin et al., On the role of AlN insertion layer in stress control of GaN on 150-mm Si (111) substrate. *Crystals* **7**(5), 134 (2017)
 20. M. Khoury et al., Evolution and prevention of meltback etching: case study of semipolar GaN growth on patterned silicon substrates. *J. Appl. Phys.* **122**(10), 105108 (2017)
 21. Y. Cordier et al., Influence of AlN growth temperature on the electrical properties of buffer layers for GaN HEMTs on silicon. *Phys. Status Solidi* **215**(9), 1700637 (2018)
 22. G. Yolcu, I. Simsek, R. Kekul, I. Altuntas, S. Horoz, I. Demir, The influence of TMGa pre-flow time and amount as surfactant on the structural and optical properties of AlN epilayer. *Micro Nanostruct.* **2022**, 207301 (2022)
 23. H. Amano et al., Metalorganic vapor phase epitaxial growth of a high quality GaN film using an AlN buffer layer. *Appl. Phys. Lett.* **48**(5), 353–355 (1986)
 24. K.M. Pürülü, M.N. Koçak, G. Yolcu, İ Perkitel, İ Altuntaş, I. Demir, Growth and characterization of PALE Si-doped AlN on sapphire substrate by MOVPE. *Mater. Sci. Semiconduct. Process.* **142**, 106464 (2022)
 25. İ Perkitel, İ Altuntas, İ Demir, The Effect of Si (111) substrate surface cleaning on Growth Rate and Crystal Quality of MOVPE grown AlN. *Gazi Univ. J. Sci.* **35**(1), 281–291 (2022)
 26. S. Hagedorn et al., AlN growth on nano-patterned sapphire: a route for cost efficient pseudo substrates for deep UV LEDs. *Phys. Status Solidi* **213**(12), 3178–3185 (2016)
 27. L. Zhang et al., High-quality AlN epitaxy on nano-patterned sapphire substrates prepared by nano-imprint lithography. *Sci. Rep.* **6**(1), 1–8 (2016)
 28. T.-Y. Wang et al., Surface evolution and effect of V/III ratio modulation on etch-pit-density improvement of thin AlN templates on nano-patterned sapphire substrates by metalorganic chemical vapor deposition. *Appl. Surf. Sci.* **455**, 1123–1130 (2018)
 29. Y. Du, B. Xu, G. Wang, Y. Miao, B. Li, Z. Kong, H.H. Radamson, Review of highly mismatched III-V heteroepitaxy growth on (001) silicon. *Nanomaterials* **12**(5), 741 (2022)
 30. M. Imura et al., High-temperature metal-organic vapor phase epitaxial growth of AlN on sapphire by multi transition growth mode method varying V/III ratio. *Jpn. J. Appl. Phys.* **45**(11R), 8639 (2006)
 31. L. Sang et al., Reduction in threading dislocation densities in AlN epilayer by introducing a pulsed atomic-layer epitaxial buffer layer. *Appl. Phys. Lett.* **93**(12), 122104 (2008)
 32. I. Demir et al., Sandwich method to grow high quality AlN by MOCVD. *J. Phys. D* **51**(8), 085104 (2018)
 33. D. Zhao et al., Parasitic reaction and its effect on the growth rate of AlN by metalorganic chemical vapor deposition. *J. Cryst. Growth.* **289**(1), 72–75 (2006)
 34. J. Bai et al., Reduction of threading dislocation densities in AlN/sapphire epilayers driven by growth mode modification. *Appl. Phys. Lett.* **88**(5), 051903 (2006)
 35. M. Imura et al., Annihilation mechanism of threading dislocations in AlN grown by growth form modification method using V/III ratio. *J. Cryst. Growth.* **300**(1), 136–140 (2007)
 36. K. Uehara et al., Growth of atomically flat-surface aluminum nitride epitaxial film by metalorganic chemical vapor deposition. *Jpn. J. Appl. Phys.* **44**(5R), 2987 (2005)

37. S. Çörekçi et al., The influence of thickness and ammonia flow rate on the properties of AlN layers. *Mater. Sci. Semiconduct. Process.* **15**(1), 32–36 (2012)
38. A. Lobanova et al., Effect of V/III ratio in AlN and AlGaN MOVPE. *J. Cryst. Growth.* **287**(2), 601–604 (2006)
39. M.N. Abd, Rahman, et al., Ammonia flux tailoring on the quality of AlN epilayers grown by pulsed atomic-layer epitaxy techniques on (0 0 0 1)-oriented sapphire substrates via MOCVD. *CrystEngComm* **21**(12), 2009–2017 (2019)
40. E. Yakovlev et al., Influence of the reactor inlet configuration on the AlGaIn growth efficiency. *J. Cryst. Growth.* **298**, 413–417 (2007)
41. A. Soltani et al., Dispersion properties and low infrared optical losses in epitaxial AlN on sapphire substrate in the visible and infrared range. *J. Appl. Phys.* **115**(16), 163515 (2014)
42. I. Demir, The contribution of AsH₃: pre-flow and V/III ratio effects on heteroepitaxially grown GaAs/Ge. *Superlattices Microstruct.* **128**, 1–8 (2019)
43. W. Tian et al., Effect of growth temperature of an AlN intermediate layer on the growth mode of AlN grown by MOCVD. *J. Phys. D* **46**(6), 065303 (2013)
44. G. Li et al., Mechanism of defects and electrode structure on the performance of AlN-based metal semiconductor metal detectors. *Mater. Res. Express* **8**(12), 125902 (2021)
45. P. Caban et al., Growth of aluminium nitride with linear change of ammonia flow. *J. Cryst. Growth.* **414**, 81–86 (2015)
46. W. Luo et al., Influence of the nucleation layer morphology on the structural property of AlN films grown on c-plane sapphire by MOCVD. *J. Alloys Compd.* **697**, 262–267 (2017)
47. M.M. Sahar et al., The Growth of AlN Single Layer on Sapphire at Low Pressure using Metalorganic Chemical Vapor Deposition (MOCVD). *Journal of Physics: Conference Series*, IOP Publishing (2020)
48. J. Marini et al., MOCVD growth of N-polar GaN on on-axis sapphire substrate: impact of AlN nucleation layer on GaN surface hillock density. *J. Cryst. Growth.* **442**, 25–30 (2016)
49. A. Shugurov, A. Panin, Mechanisms of periodic deformation of the film- substrate system under compressive stress. *Phys. Mesomech.* **13**(1–2), 79–87 (2010)
50. P. Wu et al., Control of crystal morphologies and interface structures of AlN grown on sapphire by elementary source vapor phase epitaxy. *Cryst. Growth. Des.* **16**(11), 6337–6342 (2016)
51. T. Zhang et al., Effects of growth pressure on the characteristics of the β - Ga₂O₃ thin films deposited on (0001) sapphire substrates. *Mater. Sci. Semiconduct. Process.* **123**, 105572 (2021)
52. I. Simsek, G. Yolcu, M. Koçak, K. Pürlü, I. Altuntas, I. Demir, Nucleation layer temperature effect on AlN epitaxial layers grown by metalorganic vapour phase epitaxy. *J. Mater. Sci.: Mater. Electron.* **32**(20), 25507–25515 (2021)
53. L. Chen et al., Annihilation and regeneration of defects in (112102) Semipolar AlN via High-Temperature Annealing and MOVPE Regrowth. *Cryst. Growth. Des.* **21**(5), 2911–2919 (2021)
54. M. Kuball et al., Raman scattering studies on single-crystalline bulk AlN: temperature and pressure dependence of the AlN phonon modes. *J. Cryst. Growth.* **231**(3), 391–396 (2001)
55. J. Li et al., Silane controlled three dimensional GaN growth and recovery stages on a cone-shape nanoscale patterned sapphire substrate by MOCVD. *CrystEngComm* **17**(24), 4469–4474 (2015)
56. M. Miyoshi et al., Modeling of the wafer bow in GaN-on-Si epiwafers employing GaN/AlN multilayer buffer structures. *Semicond. Sci. Technol.* **31**(10), 105016 (2016)
57. V.Y. Davydov et al., Phonon dispersion and Raman scattering in hexagonal GaN and AlN. *Phys. Rev. B* **58**(19), 12899 (1998)
58. M.N. Abd Rahman et al., Agglomeration enhancement of AlN surface diffusion fluxes on a (0 0 0 1)-sapphire substrate grown by pulsed atomic-layer epitaxy techniques via MOCVD. *CrystEngComm* **22**(19), 3309–3321 (2020)
59. M. Samsudin et al., Controlled nucleation time for improving aluminum nitride growth. *Mater. Sci. Semiconduct. Process.* **133**, 105968 (2021)

Publisher's Note Springer Nature remains neutral with regard to jurisdictional claims in published maps and institutional affiliations.

Springer Nature or its licensor (e.g. a society or other partner) holds exclusive rights to this article under a publishing agreement with the author(s) or other rightsholder(s); author self-archiving of the accepted manuscript version of this article is solely governed by the terms of such publishing agreement and applicable law.

NEW

The power of the Web of Science™ on your mobile device, wherever inspiration strikes.

Dismiss

Learn More

Find a Match

Filters [Clear All](#)

- Web of Science Coverage
- Open Access
- Category
- Country / Region
- Language
- Frequency
- Journal Citation Reports

Refine Your Search Results

JOURNAL OF MATERIALS SCIENCE-MATERIALS IN ELECTRONICS Search

Relevancy

Share These Results

JOURNAL OF MATERIALS SCIENCE-MATERIALS IN ELECTRONICS

SPRINGER, VAN GODEWIJCKSTRAAT 30, DORDRECHT, NETHERLANDS, 3311 GZ

ISSN / eISSN: 0957-4522 / 1573-482X

Science Citation Index Expanded

Current Contents Electronics & Telecommunications Collection | Current Contents Engineering, Computing & Technology | Current Contents Physical, Chemical & Earth Sciences | Essential Science Indicators

Share This Journal [View profile page](#)

** Requires free login.*

JOURNAL OF MATERIALS SCIENCE-MATERIALS IN MEDICINE OPEN ACCESS

SPRINGER, VAN GODEWIJCKSTRAAT 30, DORDRECHT, NETHERLANDS, 3311 GZ

ISSN / eISSN: 0957-4530 / 1573-4838

Science Citation Index Expanded

Current Contents Life Sciences | Essential Science Indicators

Share This Journal [View profile page](#)

** Requires free login.*

PROGRESS IN NATURAL SCIENCE-MATERIALS INTERNATIONAL

ELSEVIER SCIENCE INC, STE 800, 230 PARK AVE, NEW YORK, USA, NY, 10169

ISSN / eISSN: 1002-0071 / 1745-5391



Science Citation Index Expanded
Current Contents Physical, Chemical & Earth Sciences | Essential
Science Indicators

[Share This Journal](#) [View profile page](#)
**Requires free login.*

INFORMASIE MIDEM - JOURNAL OF MICROELECTRONICS
ELECTRONIC COMPONENTS AND MATERIALS OPEN ACCESS

SOC MICROELECTRONICS, ELECTRON COMPONENTS MATERIALS-MIDEM ,
STEGNE 7, LJUBLJANA, SLOVENIA, 1000

ISSN / eISSN: 0352-9045 / 2232-6979

Science Citation Index Expanded
Essential Science Indicators

[Share This Journal](#) [View profile page](#)
**Requires free login.*

JOURNAL OF ELECTRONIC MATERIALS

SPRINGER , ONE NEW YORK PLAZA, SUITE 4600 , NEW YORK, United States, NY,
10004

ISSN / eISSN: 0361-5235 / 1543-186X

Science Citation Index Expanded
Current Contents Electronics & Telecommunications Collection | Current
Contents Physical, Chemical & Earth Sciences | Essential Science Indicators

[Share This Journal](#) [View profile page](#)
**Requires free login.*

AES APPLIED ELECTRONIC MATERIALS

AMER CHEMICAL SOC , 1155 16TH ST, NW, WASHINGTON, USA, DC, 20036

ISSN / eISSN: 2637-6113

Science Citation Index Expanded
Current Contents Engineering, Computing & Technology | Essential
Science Indicators

[Share This Journal](#) [View profile page](#)
**Requires free login.*

ADVANCED ELECTRONIC MATERIALS OPEN ACCESS

WILEY , 111 RIVER ST, HOBOKEN, USA, NJ, 07030-5774

ISSN / eISSN: 2199-160X

Science Citation Index Expanded

Current Contents Physical, Chemical & Earth Sciences | Essential Science Indicators

[Share This Journal](#)

[View profile page](#)

**Requires free login.*

ELECTRONIC MATERIALS LETTERS

KOREAN INST METALS MATERIALS , KIM BLDG 6TH FLOOR, SEOCHO-DAERO 56 GIL 38, SEOCHO-GU, SEOUL, SOUTH KOREA, 137-881

ISSN / eISSN: 1738-8090 / 2093-6788

Science Citation Index Expanded

Essential Science Indicators

[Share This Journal](#)

[View profile page](#)

**Requires free login.*

TRANSACTIONS ON ELECTRICAL AND ELECTRONIC MATERIALS

SPRINGER , ONE NEW YORK PLAZA, SUITE 4600 , NEW YORK, United States, NY, 10004

ISSN / eISSN: 1229-7607 / 2092-7592

Emerging Sources Citation Index

[Share This Journal](#)

[View profile page](#)

**Requires free login.*

ACS MATERIALS AU

OPEN ACCESS

Publisher: AMER CHEMICAL SOC , 1155 16TH ST, NW, WASHINGTON, USA, DC, 20036

ISSN / eISSN: 2694-2461

Emerging Sources Citation Index

[Share This Journal](#)

[View profile page](#)

**Requires free login.*

Items per page: 10 ▾ 1 - 10 of 1531 |< < > >|

Subject

5



Clarivate.™ Accelerating innovation.

© 2023 Clarivate

[Legal center](#)

[Privacy notice](#)

[Cookie policy](#)

[Tanımlama Bilgisi Ayarları](#)

[Copyright notice](#)

[Help](#)

